J Mater Sci (2021) 56:14866–14879

Polymers & biopolymers

Facile preparation of three-dimensional graphene oxide/ι-carrageenan composite aerogel and its efficient ability for selective adsorption of methylene blue

Guobin Song[1], Yawei Shi[1], Anqi Li[1], Haonan Wang[1], and Guanghui Ding[1,*]

[1] College of Environmental Science and Engineering, Dalian Maritime University, Linghai Road 1, Dalian 116026, P. R. China

Received: 9 February 2021
Accepted: 25 May 2021
Published online: 14 June 2021

ABSTRACT

A three-dimensional graphene oxide/ι-carrageenan composite aerogel (GO/ι-Car) has been facilely manufactured in a benign approach and characterized in detail. The adsorption ability of the GO/ ι-Car aerogel was also investigated on the methylene blue (MB) removal from synthesized solutions. It was found that the adsorption process followed the pseudo-second-order kinetic model. The Langmuir maximum adsorption capacity of MB on the GO/ι-Car aerogel was calculated to be 245.28 mg g^{-1}. Thermodynamic calculations proved that the adsorption was a spontaneous, exothermic process with the enthalpy change of −10.36 kJ mol^{-1} and the entropy change of 54.64 J mol^{-1} K^{-1}. Furthermore, adsorption selectivity studies showed that the GO/ ι-Car aerogel could selectively adsorb the cationic MB in the presence of anionic dye methyl orange, which was mainly attributed to the electrostatic attraction between the negatively charged aerogel and the positively charged MB. In addition, the MB removal rate by the GO/ι-Car aerogel could still reach 91.9% after three desorption–adsorption cycles. Overall, the GO/ι-Car aerogel prepared in this study could be a green, cost-effective, reusable and promising selective adsorbent for cationic dye removal from water.

Introduction

With the mass production and wide application of dyes, the printing and dyeing wastewater has become one of the main pollution sources, which seriously endangers the lives of animals and plants and eventually leads to great harm to the entire food chain [1]. Among various dyes, methylene blue (MB) (Scheme 1a) as a typical and widely used cationic dye could lead to serious harm to human health [2]. Treatment technologies, including biological

Handling Editor: Lisa White.

Guobin Song and Yawei Shi contributed equally.

Address correspondence to E-mail: guanghuiding@dlmu.edu.cn

https://doi.org/10.1007/s10853-021-06211-7

treatment [3], flocculation precipitation [4], membrane separation [5], redox [6], photocatalytic degradation [7], ion exchange [8] and adsorption, have been utilized for the treatment of the dye wastewater. Among them, adsorption is known as a popular approach due to its high efficiency, simple operation and low cost [9, 10]. Therefore, various novel adsorbents have been developed and used on the adsorption removal of dyes from the printing and dyeing wastewater, such as clays, zeolites and their composites, biosorbents, agricultural solid wastes, metal organic frameworks and carbonaceous nanomaterials [11].

In the past decades, graphene oxide (GO) as an important derivative of graphene has attracted increasing attention on the adsorption [11, 12]. The existence of abundant functional groups, such as carboxyl (–COOH) and hydroxyl (–OH), endowed GO the ability to interact with water molecules through hydrogen bonding, showing high hydrophilicity [13]. Moreover, the large surface area and abundant oxygen-containing functional groups have endowed GO excellent adsorption ability to remove organic dyes from water [14]. However, the high colloidal stability of GO sheets makes it hard to collect them after the adsorption [15], hindering potential practical applications. To address this issue, magnetic separation as an excellent separation technology has been utilized, where magnetic adsorbents can be facilely separated using an external magnetic field within several seconds or minutes [16]. However, the preparation process for magnetic adsorbents was usually complicated and the magnetism gradually decreased after the repeated use. Besides, secondary pollution could be caused through leaching metal species into water under acid conditions.

Recently, three-dimensional GO-based materials, such as anionic polyacrylamide/GO aerogels [17], agar/GO [18] and lignosulfonate/GO composite aerogels [19], have been constructed through incorporation of polymers to GO sheets with the assistance of cross-linking agents, which were used on the adsorption removal of dyes from water. These GO-based aerogels have high pore volumes, large surface areas and abundant oxygen-containing functional groups and thus generally show large adsorption capacities for dyes. In addition, they could be easily separated from water after use [20]. For the preparation of GO-based aerogels, polysaccharide biopolymer is often used.

Polysaccharide biopolymer materials have attracted widespread attention due to their unique renewable, non-toxic, low cost, biocompatible and biodegradable properties. Carrageenan is a family of linear sulfated polysaccharides that are obtained by alkaline extraction from some species of red seaweeds, which has been widely used as gelling agent, thickener and stabilizer in many fields. Among them, *ι*-carrageenan (Scheme 1b) is a hydrophilic colloid with a long-chain structure and high stability [21]. Each disaccharide unit of *ι*-carrageenan has two sulfonate groups, which can interact with cationic dyes [22]. The ability of carrageenan to interact with cationic dyes [23] and its gelling property make it a promising participant for preparing GO-based aerogels, which are used for the dye adsorption [24].

Therefore, in the present study, natural polysaccharide of *ι*-carrageenan and GO are employed to prepare a kind of novel GO-based aerogel, which is subsequently used for the dye adsorption. The integration of polysaccharide long-chains and GO nanosheets resulted in a porous aerogel composite, which could be facilely separated from water after the adsorption. A gentle and simple synthesis approach is applied to avoid severe changes of the oxygen-containing functional groups on the surface of GO, and the whole process is free of any toxic

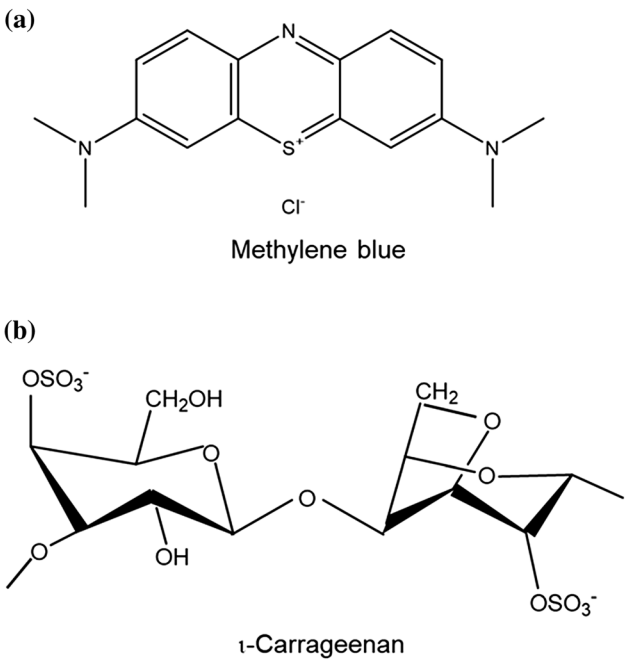

Scheme 1 Structure of methylene blue (**a**) and repeated disaccharide unit of *ι*-carrageenan (**b**).

polymer or cross-linking agent. In this study, MB was chosen as a typical organic dye in water and its adsorption behavior on the GO/ι-Car aerogel was investigated in detail.

Experimental

Chemicals

GO was purchased from Chengdu Organic Chemistry Co., Ltd., and its detailed properties are listed in Table S1 of Supplementary Materials. ι-carrageenan and methylene blue (MB) were obtained from J&K Scientific Ltd. Ethanol, HCl (36.0–38.0%), NaOH (≥ 96.0%) and alkyl glycoside (APG) were supplied from Tianjin Damao Chemical Reagent Co., Ltd. Deionized water was used throughout the experiments.

Preparation and characterization of GO/ι-Car aerogel

In a typical synthesis, a given amount of APG (1% v/v) was added dropwise into 20 mL of dispersed GO solution (4 mg mL^{-1}) with continuous stirring for 30 min. Here, APG is a natural green non-ionic surfactant prepared by dehydration condensation of starch or its hydrolyzed sugar with fatty alcohol. The mixture was then heated at 80 °C while adding 16 mg of ι-carrageenan and stirred for another 1 h until completely dissolved. After heating, the mixture was cooled at room temperature to form a hydrogel. Then, the as-prepared material was put in a refrigerator at -20 °C for 4 h and freeze-dried for 24 h to obtain the GO/ι-Car aerogel. Actually, it was found that increasing the GO/ι-Car ratio could enhance the removal of MB, but the aerogel prepared at a ratio larger than 5:1 was not stable enough and would collapse after the adsorption. Therefore, the mass ratio of GO to ι-carrageenan was fixed at 5:1. The GO/ι-Car aerogel was washed with deionized water before its use for the adsorption.

The aerogel was characterized by scanning electron microscopy (SEM), Fourier transform infrared spectrometer (FTIR), thermogravimetric analysis (TGA), X-ray diffraction (XRD), X-ray photoelectron spectroscopy (XPS) and zeta potential measurements. Details for the methods of characterization are provided in Text S1 of Supplementary Materials.

Adsorption of single MB

Batch experiments were conducted for MB adsorption on GO/ι-Car aerogel. For comparison, the adsorption performance of raw ι-carrageenan was also tested and is discussed in Text S2. The remaining MB concentration after the adsorption was determined at 664 nm with a UV–Vis spectrophotometer (Sunny Hengping Scientific Instrument Co., Ltd., China). Kinetic studies were performed by fitting the data to the pseudo-first-order kinetic model [25], pseudo-second-order kinetic model [26] and intraparticle diffusion model [27]. Adsorption isotherms were fitted with the Langmuir model [28] and Freundlich model [29]. Thermodynamic analysis was conducted by calculating Gibbs free energy change (ΔG^0), enthalpy change (ΔH^0) and entropy change (ΔS^0) [30, 31]. More details are provided in Text S3 of Supplementary Materials.

Selective adsorption for cationic and anionic dyes

In order to test the selective removal ability of the aerogel, 5 mg of GO/ι-Car was soaked into 20 mL of MB/MO mixed solution ($C_{MB} = C_{MO} = 10$ mg L^{-1}). The mixed solution was prepared by physical mixing 20 mg L^{-1} MB solution with 20 mg L^{-1} MO solution in equal volume. The mixed solutions were sampled at different time intervals after the adsorption, and absorbances were measured at 664 and 464 nm by using the UV–Vis spectrometer. Concentrations of MB and MO in the mixed solutions were calculated by solving the corresponding binary linear equations, which are provided in Text S4 of Supplementary Materials.

Reuse of GO/ι-Car aerogel

In order to investigate the reusability of the GO/ι-Car aerogel, 25 mg of GO/ι-Car aerogel was firstly added into a conical flask containing 25 mL of MB aqueous solution (100 mg L^{-1}). After the adsorption for 480 min, the GO/ι-Car aerogel was separated from the aqueous solution and was regenerated with 0.1 M HCl for several times. Subsequently, the desorption and adsorption processes were repeated three cycles and changes of the removal rate were analyzed.

Results and discussion

Characterization of GO/ι-Car

The morphologies of GO and GO/ι-Car were analyzed by SEM (Fig. 1). SEM images of GO (Fig. 1a, b) exhibit a typical two-dimensional structure with many wrinkles [32]. The GO/ι-Car aerogel composite (Fig. 1c, d) exhibited a three-dimensional porous structure, which resulted from the connection of ι-carrageenan long chains and GO.

GO, ι-carrageenan and the GO/ι-Car aerogel were further analyzed by FTIR (Fig. 2). The broad band at 3200–3500 cm^{-1} can be found in all spectra due to the abundant hydroxyls present in all three samples. In the spectrum of GO, bands appear at 1731, 1621, 1055 and 1386 cm^{-1}, which are attributed to C = O, C = C, C–O stretching and C–H deformation vibrations [33]. For ι-carrageenan, bands for C–H stretching vibration at 2933 cm^{-1} and C–O–C stretching vibration at 1159, 1075 and 930 cm^{-1} were observed [34, 35]. In addition, the bands at 1029 and 1267 cm^{-1} were associated with glycosidic linkages [36] and O = S = O stretching [34, 37], respectively. GO/ι-Car exhibited both bands of GO and ι-carrageenan with slightly shifted wavenumbers, which was possibly due to structural changes between free and GO-bonded ι-carrageenan. The spectrum of GO/ι-Car + MB was also analyzed for the sample of GO/ι-Car aerogel after the MB adsorption. Bands in the spectrum at 1598, 1489, 1338 and 885 cm^{-1} indicated that MB had been adsorbed by the aerogel successfully [38].

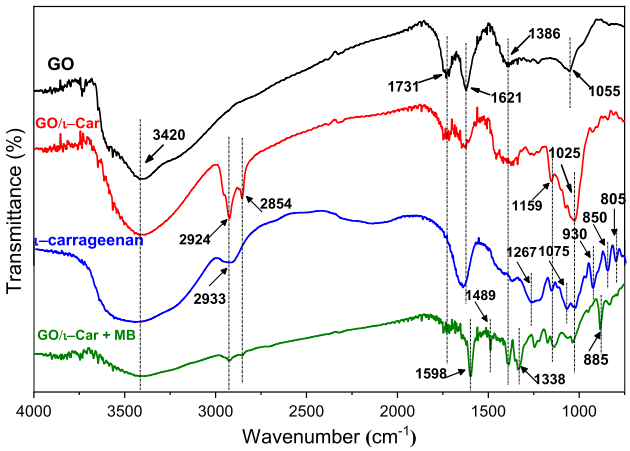

Figure 2 FTIR spectra of GO, ι-carrageenan, GO/ι-Car and GO/ι-Car-MB.

The behaviors of GO, ι-carrageenan and GO/ι-Car aerogel under the heat treatment were also analyzed. As shown in Fig. 3, the weight of carrageenan decreased drastically below 185 °C, losing 23.1% of its weight. This was due to the weight loss caused by the volatilization of water, and the residual weight at 800 °C was 29.0% (losing 71.0%). TGA curves of GO and GO/ι-Car aerogel were similar and could be divided into three main stages. The first stage was the

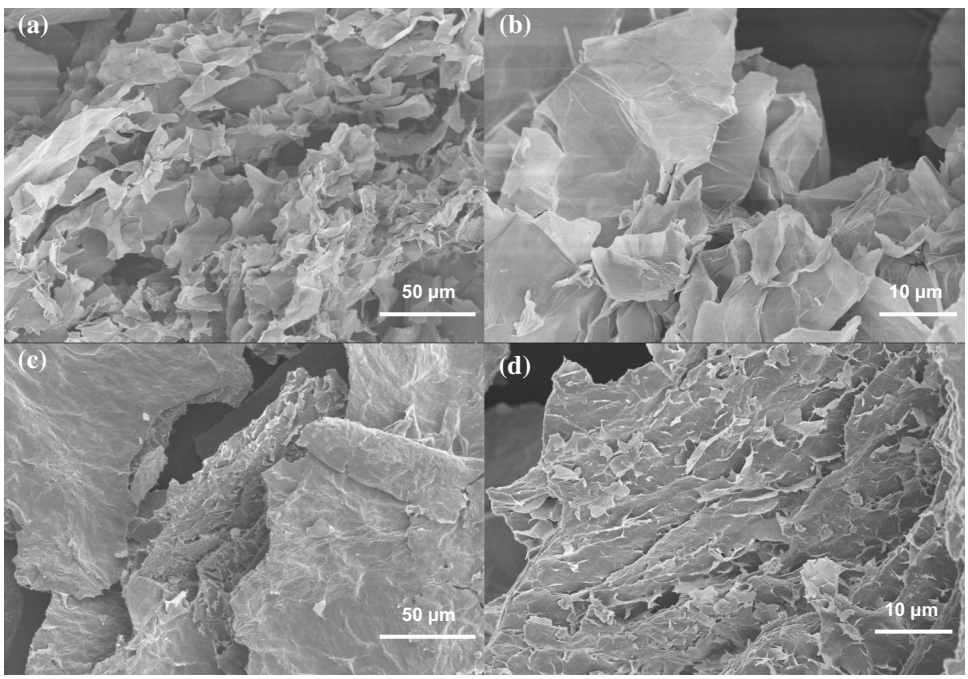

Figure 1 SEM images of GO (**a**, **b**) and the GO/ι-Car aerogel (**c**, **d**) at different magnifications.

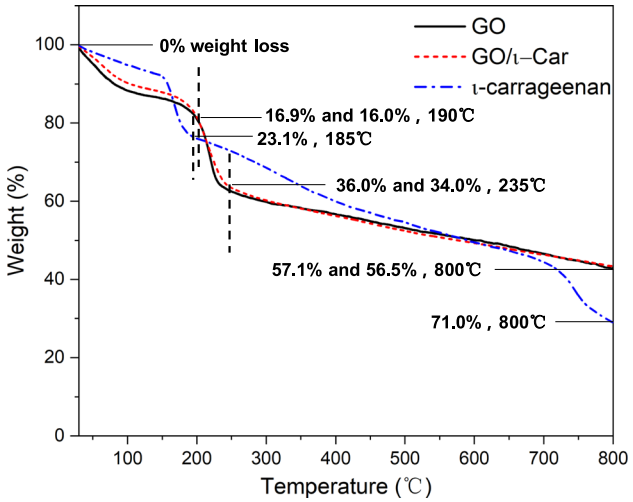

Figure 3 TGA curves of GO, *ι*-carrageenan and GO/*ι*-Car.

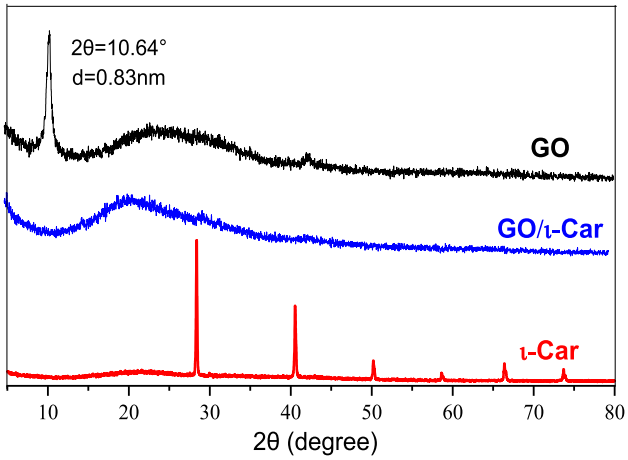

Figure 4 XRD patterns of GO, *ι*-carrageenan and GO/*ι*-Car aerogel.

weight loss of adsorbed water below 190 °C [39]. Percentages of the weight loss of GO and GO/*ι*-Car aerogel were 16.9% and 16.0%, respectively. The second stage was a rapid weight-losing stage between 190 °C and 235 °C, during which the functional groups decomposed [40]. Percentages of the weight loss of GO and GO/*ι*-Car aerogel were 19.1% and 18.0%, respectively. The third stage was ascribed to the decomposition of more stable functional groups, and the final residual weights were 42.9% and 43.5% for GO and GO/*ι*-Car aerogel, respectively. As GO accounts for a much larger proportion than *ι*-carrageenan in the composite aerogel, the TGA curve of GO/*ι*-Car was more similar to that of GO [18].

Figure 4 displays XRD patterns of GO, *ι*-carrageenan and the GO/*ι*-Car aerogel. For GO, a strong diffraction peak appeared at $2\theta = 10.64°$, which was the characteristic diffraction peak of GO. The layer spacing (d) of GO was calculated to be 0.83 nm according to the Bragg's law [41]. The diffraction peaks observed in the pattern of *ι*-carrageenan were attributed to KCl impurity (JCPDS 41-1476) [42]. For the GO/*ι*-car aerogel, the diffraction peak of GO completely disappeared, indicating that GO sheets were well exfoliated in the composite aerogel [43]. There were no diffraction peaks existed as those appeared for *ι*-carrageenan, which might be related to the washing away of KCl impurity during the preparation of the GO/*ι*-Car aerogel.

XPS spectra were used to characterize their surface functional groups (Fig. 5). Survey scans of GO and GO/*ι*-Car (Fig. 5a, d) possessed obvious C1s and O1s peaks. In the C1s spectra (Fig. 5b, e), three peaks were ascribed to carbon in C = O, C–O and C–C & C = C bonds [44]. In the O1s spectra (Fig. 5c, f), oxygen in C–O and C = O bonds were indicated as two peaks [45]. As shown in Table S2, the contribution of C–O in C1s spectrum of GO/*ι*-Car increased significantly, which was due to the introduction of a large number of hydroxyl groups by the polysaccharide molecules. The reduction of graphene oxide during the preparation process might occur, but the result here indicated that its contribution was not enough to offset the increase of hydroxyl groups. The increased contribution from C–O was also observed from the O1s spectra (Fig. 5c, f and Table S2), supporting the above conclusion.

Effects of pH and adsorbent dosage on MB adsorption

The effect of pH on the MB adsorption by GO/*ι*-Car aerogel is illustrated in Fig. 6a. The removal rate rose with increasing pH values. Similar pH effects were observed for the MB removal using other adsorbents such as poly (c-glutamic acid) [46] and alginate [47]. The increased MB adsorption amounts at high pH values were due to less competition between H^+ and MB and the more significant deprotonation of functional groups on the surface of GO/*ι*-Car [48]. As shown in Table S3, negative zeta potentials were observed for the GO/*ι*-Car aerogel, and the absolute values increased with increasing pH. The interaction between the aerogel and MB molecules is non-covalent interaction, i.e., electrostatic and π–π interaction

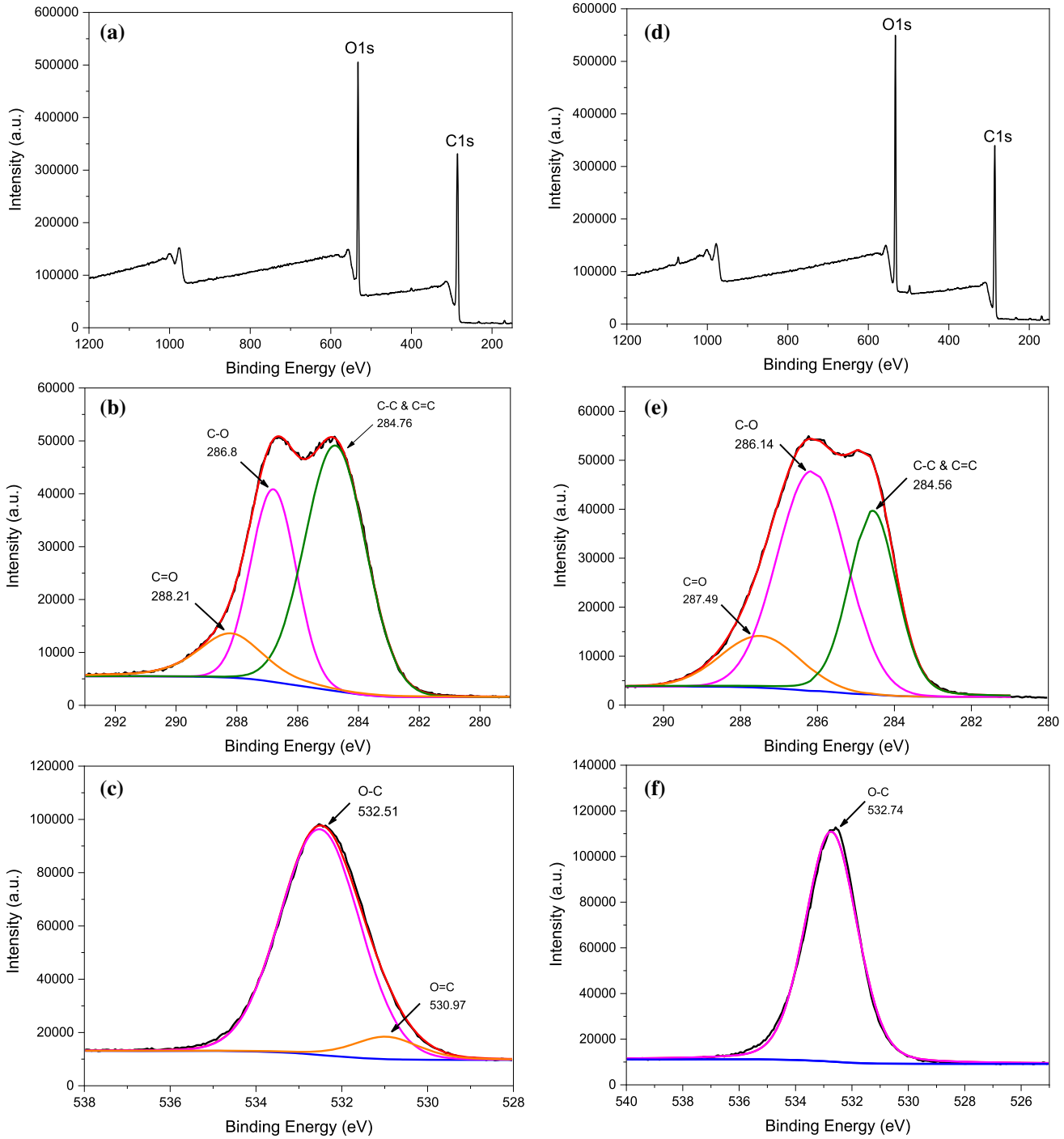

Figure 5 XPS spectra of GO (a, b and c) and GO/*ι*-Car (d, e and f).

[49]. At higher pH, stronger electrostatic attraction between the negatively charged carboxyl, hydroxyl and sulfonic acid groups and the positively charged MB cations resulted in a larger adsorption amount.

Figure 6b shows the effect of GO/*ι*-Car aerogel dosage on the MB adsorption. With increasing dosages, the removal rate of MB increased first and then remained almost unchanged. At a higher aerogel dosage, the amount of available adsorption sites increased, leading to a higher removal rate until almost complete removal of MB was achieved. From Fig. 6b, the optimal dosage was determined to be 1.0 g L^{-1}.

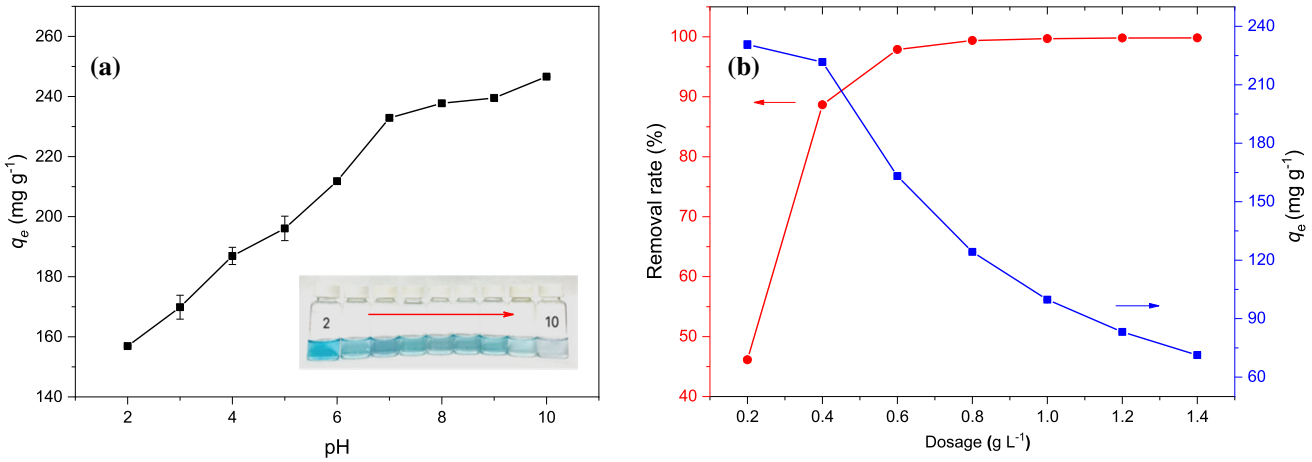

Figure 6 Effects of pH (**a**) and GO/*ι*-Car aerogel dosage (**b**) on the MB adsorption (adsorption conditions: dosage = 0.4 g L^{-1}, C_0 = 100 mg L^{-1}, T = 298 K, t = 240 min (**a**); C_0 = 100 mg L^{-1}, T = 298 K, pH = 7, t = 240 min (**b**)).

Adsorption kinetics

The effect of adsorption time at initial MB concentrations of 100, 200 and 400 mg L^{-1} is shown in Fig. 7a. The adsorption curve showed a rapid adsorption in initial 60 min, which was ascribed to a large number of adsorption sites on the surface of GO/*ι*-Car aerogel [50]. The decrease of adsorption rate with prolonged time was due to the reduction of the MB concentration gradient between the two phases.

The kinetic parameters obtained by nonlinear fitting to the pseudo-first-order kinetic model (Fig. 7b) and pseudo-second-order kinetic model (Fig. 7c) models are shown in Table 1. Coefficients of determination (R^2) of the latter model were higher, and the calculated adsorption amounts were closer to the corresponding experimental values (q_{exp}). Therefore, the pseudo-second-order kinetic model performed better for the description of MB adsorption behavior on the GO/*ι*-Car aerogel compared to the pseudo-first-order kinetic model.

The intra-particle diffusion model was also used (Fig. 7d and Table 2). The adsorption curve can be divided into three linear segments, indicating three adsorption stages. At the initial stage, there were abundant adsorption sites available on the surface of GO/*ι*-Car aerogel, and the adsorption proceeded quickly. With the adsorption going on, the amount of adsorption sites gradually decreased, and MB molecules gradually formed a boundary layer, resulting in declined adsorption rate [51]. The final stage involved diffusion of MB molecules into pores and pore-wall surfaces of the GO/*ι*-Car aerogel until the saturation stage reached.

Adsorption isotherms

The nonlinear fitting results of Langmuir and Freundlich isotherms are shown in Fig. 8, and the corresponding parameters are listed in Table 3. The results showed that high R^2 was obtained for these two models, indicating both models could describe the adsorption process. As R^2 of the Freundlich model was higher than that of the Langmuir model, the adsorption might follow the multilayer adsorption and heterogeneity distribution mechanism [29].

The maximum adsorption capacity (q_m) of MB on the GO/*ι*-Car aerogel was calculated to be 245.28 mg g^{-1} from Langmuir model. As shown in Table 4, the GO/*ι*-Car aerogel showed higher or comparable adsorption capacity of MB than reported values, including graphene aerogel [52], Fe_3O_4/RGO aerogel [53] and CMC/chitosan/GO [54]. Although such comparisons may not be sufficient enough due to different experimental conditions such as pH value and temperature, the result here suggested that the GO/*ι*-Car aerogel prepared may be an economical and efficient green adsorbent for removal of cationic dyes such as MB.

Adsorption thermodynamics

Thermodynamic parameters were obtained from the Van't Hoff diagram (Fig. S1). As shown in Table 5, the value of ΔG^0 was negative at all temperatures,

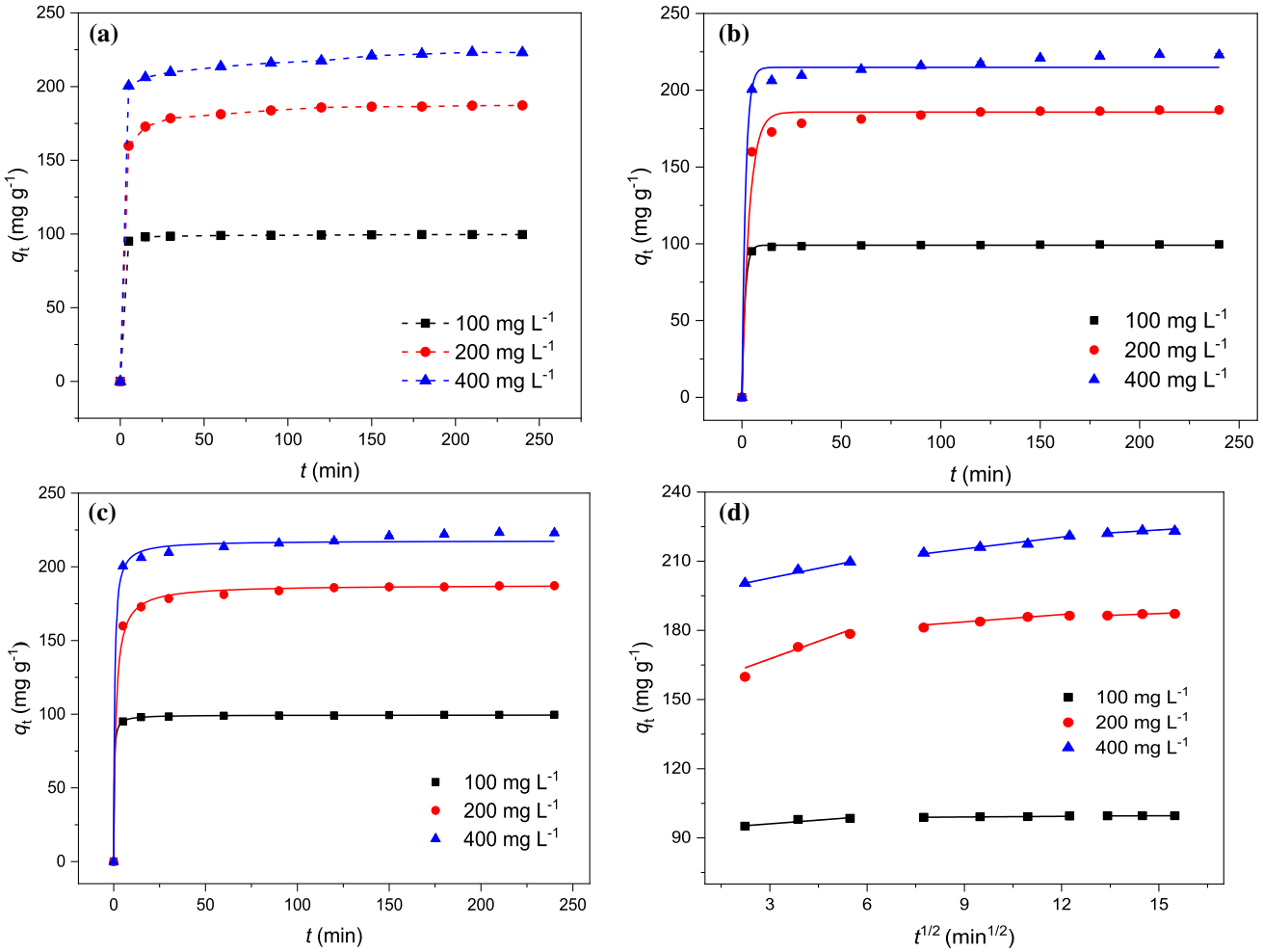

Figure 7 Effect of contact time on MB adsorption capacity (**a**), pseudo-first-order kinetic model (**b**), pseudo-second-order kinetic model (**c**) and intra-particle diffusion model (**d**) for MB adsorption on GO/*ι*-Car aerogel (adsorption conditions: dosage = 1.0 g L^{-1}, T = 298 K, pH = 7, t = 0 ~ 240 min).

Table 1 The parameters of pseudo-first-order kinetic model and pseudo-second-order kinetic model for MB adsorption on GO/*ι*-Car aerogel

C_0 mg L^{-1}	q_{exp} mg g^{-1}	Pseudo-first-order kinetic model			Pseudo-second-order kinetic model		
		k_1 min^{-1}	q_e mg g^{-1}	R^2	k_2 10^{-2} g (mgmin)$^{-1}$	q_e mg g^{-1}	R^2
100	99.43	0.641	99.10	0.919	4.342	99.45	0.988
200	187.17	0.274	185.79	0.922	0.454	187.74	0.995
400	223.21	0.540	214.89	0.888	0.885	217.77	0.932

indicating that the adsorption of MB on the GO/*ι*-Car aerogel was spontaneous. As the temperature increased, the absolute value of ΔG^0 increased as well. The value of ΔH^0 was negative, indicating that the adsorption process of MB on the GO/*ι*-Car aerogel was an exothermic process, which was in accordance with the experimental result that the adsorption amount of MB decreases with increasing temperature. The adsorption of MB molecules led to freedom loss and thus decreased entropy, while desorption of water molecules, which occurred at the same time [59] and change the adsorbent surface,

Table 2 The parameters of intra-particle diffusion model for MB adsorption on GO/*t*-Car aerogel

C_0 mg L^{-1}	Stage I			Stage II			Stage III		
	k_{i1} mg $(g{\cdot}min^{1/2})^{-1}$	C_{i1}	R^2	k_{i2} mg $(g{\cdot}min^{1/2})^{-1}$	C_{i2}	R^2	k_{i3} mg $(g{\cdot}min^{1/2})^{-1}$	C_{i3}	R^2
100	1.070	92.89	0.912	0.093	98.22	0.922	0.016	99.33	0.912
200	5.077	152.41	0.884	1.065	174.10	0.838	0.521	179.50	0.882
400	2.838	194.17	0.998	1.701	200.03	0.991	0.843	210.93	0.796

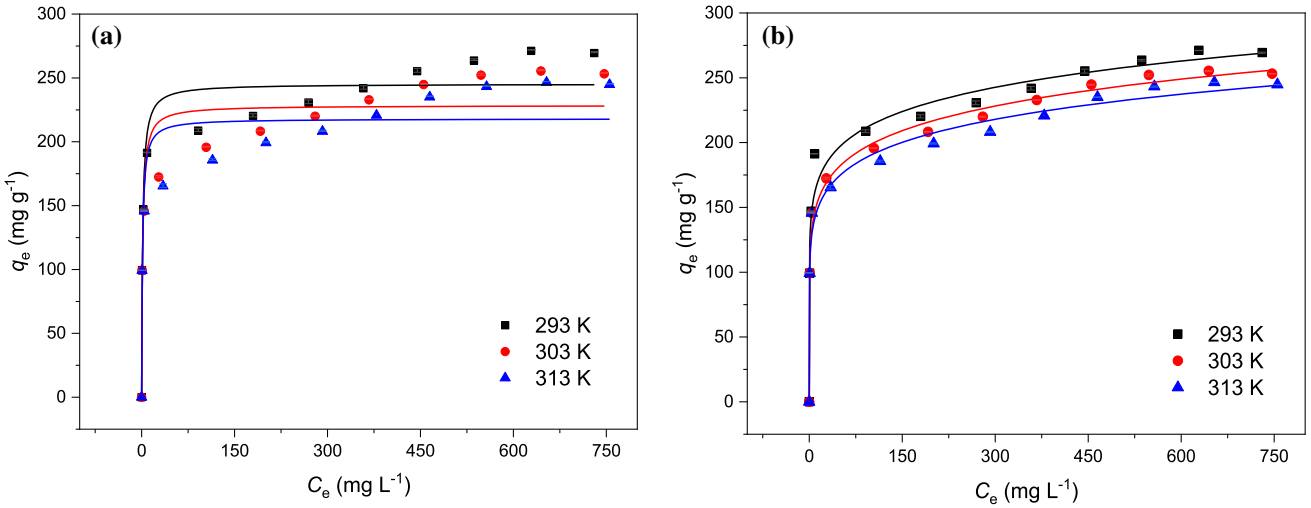

Figure 8 Langmuir isotherm (**a**) and Freundlich isotherm (**b**) for the adsorption of MB onto the GO/*t*-Car aerogel (adsorption conditions: dosage = 1.0 g L^{-1}, t = 480 min, pH = 7, C_0 = 100 ~ 1000 mg L^{-1}).

Table 3 The parameters of Langmuir and Freundlich isotherm for MB adsorption on GO/*t*-Car aerogel

T	Langmuir			Freundlich		
K	q_m mg g^{-1}	K_L L g^{-1}	R^2	$1/n$	K_F (mg g^{-1})·(L mg^{-1})$^{1/n}$	R^2
293	245.28	0.594	0.934	0.116	125.46	0.975
303	228.46	0.602	0.885	0.126	111.50	0.993
313	218.03	0.703	0.876	0.123	108.15	0.988

Table 4 The adsorption capacity of MB on various adsorbents

Adsorbent	Adsorption capacity (mg g^{-1})	pH	T (K)	Reference
Graphene aerogel (GA15)	88.00	5.0	298	[52]
Fe_3O_4/RGO aerogel	163.80	7.0	298	[53]
RCE/GO aerogel	68.00	6.0	298	[55]
CMC/graphene oxide hydrogel	58.24	6.0	293	[56]
CMC/chitosan/GO nanocomposite	122.10	7.0	298	[54]
PCMC/acrylic acid/acrylamide/GO hydrogels	133.32	7.0	-	[57]
CMC/GOCOOH composite microbeads	180.23	8.0	298	[58]
GO/*t*-Car aerogel	245.28	7.0	293	This study

Table 5 The parameters of adsorption thermodynamics for MB adsorption on the GO/*ι*-Car aerogel

T (K)	$\triangle G^0$ (kJ mol^{-1})	$\triangle H^0$ (kJ mol^{-1})	$\triangle S^0$ (J mol^{-1} K^{-1})
293	− 25.37	− 10.36	54.64
303	− 26.92		
313	− 27.46		

resulted in increased entropy [60]. The positive ΔS^0 indicated the net disorder increase in the whole adsorption process.

Selective adsorption

To investigate the adsorption selectivity of GO/*ι*-Car aerogel for cationic dyes, MO as a typical anionic dye was mixed with MB and the adsorption of MB from mixed dye solutions was investigated (Fig. 9). At pH = 7, the removal rate of MB approached 90% at 240 min, while MO was only removed by about 6%. The inserted picture in Fig. 9 shows the color change from green (the color of the mixed solution of MB and MO) to orange after the adsorption, which also verified the selective removal of MB. This result was mainly attributed to the electrostatic attraction between cationic dye MB and the negatively charged functional groups on the surface of GO/*ι*-Car aerogel. In contrast, the anionic dye MO was expected to suffer electrostatic repulsion, resulting in a very low removal rate. Therefore, the GO/*ι*-Car aerogel prepared in this study could selectively adsorb cationic rather than anionic dyes, showing some potential for practical applications on the dye separation.

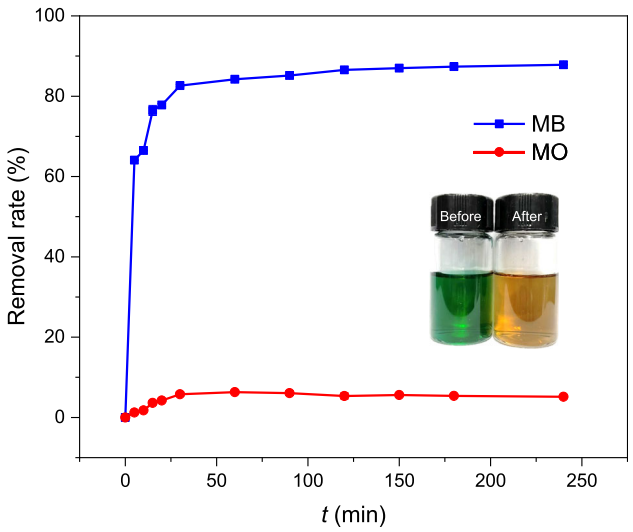

Figure 9 The corresponding removal rate of MB/MO mixture by the GO/*ι*-Car aerogel (adsorption conditions: dosage = 0.25 g L^{-1}, $C_{MB} = C_{MO}$ = 10 mg L^{-1}, T = 298 K, pH = 7).

In order to better understand the adsorption mechanism, schematic diagrams are provided in Fig. 10 based on previous reports [12, 61, 62] and the results of this study. Generally, electrostatic interaction, π–π stacking and hydrophobic interaction were involved for the adsorption. Particularly, the positively charged MB cation tended to interact with the GO/*ι*-Car aerogel which possessed negatively charged carboxyl, hydroxyl and sulfonic acid groups mainly through electrostatic attraction (Fig. 10a). For the adsorption of MO (Fig. 10b), the negatively charge on MO molecules would cause electrostatic repulsion from the GO/*ι*-Car aerogel, resulting in limited adsorption amount. Consequently, the GO/*ι*-Car aerogel was more favorable for the adsorption of MB than MO.

Desorption and reuse of the adsorbent

The reusability is of great importance for an adsorbent. After the adsorption at initial MB concentration of 100 mg L^{-1}, adsorbent dosage of 1 g L^{-1} and adsorption time of 480 min, the GO/*ι*-Car aerogel was separated from the solution and was regenerated with 0.1 M HCl for several times. Images of the color change of the solutions during the adsorption–desorption process are shown in Fig. S3, indicating the efficient desorption of MB from the GO/*ι*-Car aerogel used. In addition, from Fig. 11, it can be seen that the removal rate remained at a satisfactory level and could still reach 91.9% after three desorption–adsorption cycles. Therefore, GO/*ι*-Car aerogel could be a reusable and effective adsorbent for the cationic dye removal.

Conclusion

A novel three-dimensional GO/*ι*-Car composite aerogel was prepared in a facile and green approach and then employed as an adsorbent for MB removal

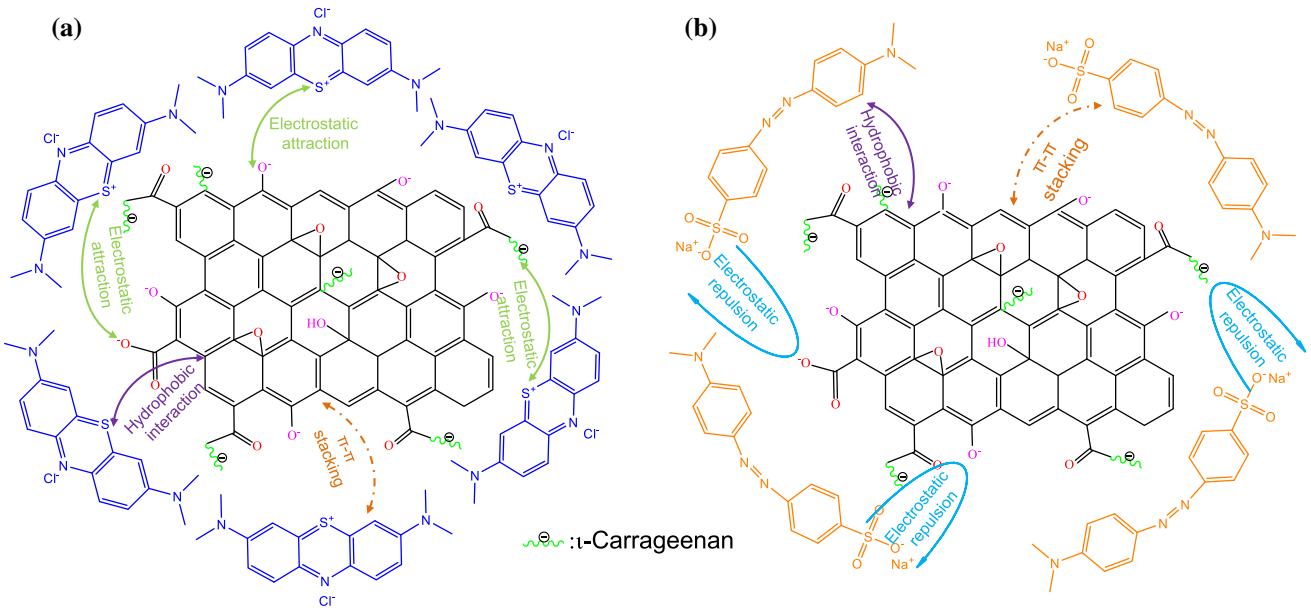

Figure 10 Adsorption mechanisms of MB (**a**) and MO (**b**) on the GO/*ι*-Car aerogel.

from water. Kinetic studies showed that the adsorption process followed the pseudo-second-order kinetic model. According to isotherm studies, the maximum adsorption capacity of MB on the GO/*ι*-Car at 293 K was calculated to be 245.28 mg g^{-1}, which was higher or comparable to those values of reported adsorbents. Thermodynamic calculations proved that the adsorption was a spontaneous, exothermic process with the enthalpy change of -10.36 kJ mol^{-1} and the entropy change of 54.64 J mol^{-1} K^{-1}. More importantly, the aerogel could selectively adsorb MB in the MB/MO mixed solution, which was attributed to the electrostatic attraction between the negatively charged aerogel and the positively charged MB. The MB removal rate by the GO/ *ι*-Car aerogel could still reach 91.9% after three desorption–adsorption cycles. Therefore, the GO-based aerogel prepared in this study has potential applications for the cationic dye adsorption and dye separation from water.

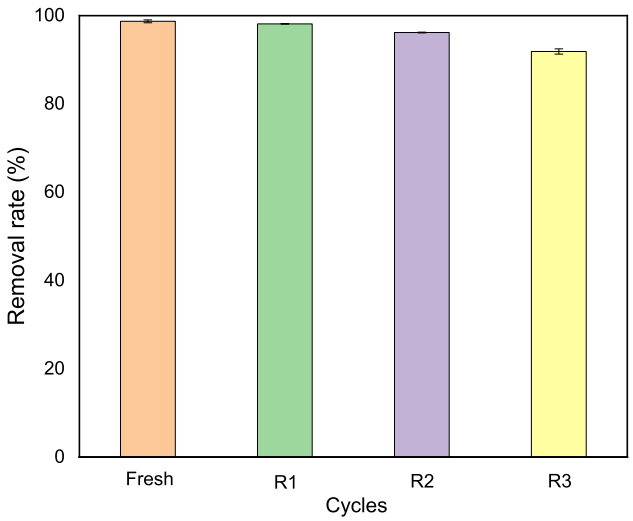

Figure 11 Removal rates of MB by the GO/*ι*-Car aerogel in different cycles.

Acknowledgements

This work was financially supported by the Joint Research Fund Liaoning-Shenyang National Laboratory for Materials Science (20180510004) and the National Natural Science Foundation of China (51479016, 51908409).

Author contributions

GS was involved in methodology, data curation, investigation and writing—original draft. YS was involved in writing—review and editing. AL was involved in formal analysis and data curation. HW

was involved in investigation, visualization and formal analysis. GD was involved in writing—review and editing, conceptualization, resources and supervision.

Declarations

Conflict of interest The authors declare that they have no known competing financial interests or personal relationships that could have appeared to influence the work reported in this paper.

Supplementary Information: The online version contains supplementary material available at https://doi.org/10.1007/s10853-021-06211-7.

References

[1] Xu H, Yang B, Liu Y, Li F, Shen C, Ma C, Tian Q, Song X, Sand W (2018) Recent advances in anaerobic biological processes for textile printing and dyeing wastewater treatment: a mini-review. World J Microbiol Biotechnol 34:165

[2] Manna S, Roy D, Saha P, Gopakumar D, Thomas S (2017) Rapid methylene blue adsorption using modified lignocellulosic materials. Process Saf Environ 107:346–356

[3] Alvarez MS, Moscoso F, Rodriguez A, Sanroman MA, Deive FJ (2013) Novel physico-biological treatment for the remediation of textile dyes-containing industrial effluents. Bioresour Technol 146:689–695

[4] Verma AK, Dash RR, Bhunia P (2012) A review on chemical coagulation/flocculation technologies for removal of colour from textile wastewaters. J Environ Manage 93:154–168

[5] Wang J, Wu Z, Li T, Ye J, Shen L, She Z, Liu F (2018) Catalytic PVDF membrane for continuous reduction and separation of p-nitrophenol and methylene blue in emulsified oil solution. Chem Eng J 334:579–586

[6] Li B, Dong Y, Zou C, Xu Y (2014) Iron (III)-alginate fiber complex as a highly effective and stable heterogeneous fenton photocatalyst for mineralization of organic dye. Ind Eng Chem Res 53:4199–4206

[7] Pethsangave DA, Khose RV, Wadekar PH, Kulal DK, Some S (2020) One-Pot synthetic approach for magnetically separable graphene nanocomposite for dye degradation. ChemistrySelect 5:1516–1525

[8] Li L, Qi G, Wang B, Yue D, Wang Y, Sato T (2018) Fulvic acid anchored layered double hydroxides: a multifunctional composite adsorbent for the removal of anionic dye and toxic metal. J Hazard Mater 343:19–28

[9] Zbair M, Anfar Z, Khallok H, Ahsaine HA, Ezahri M, Elalem N (2018) Adsorption kinetics and surface modeling of aqueous methylene blue onto activated carbonaceous wood sawdust. Fuller Nanotub Car N 26:433–442

[10] Hosseini SM, Shahrousvand M, Shojaei S, Khonakdar HA, Asefnejad A, Goodarzi V (2020) Preparation of superabsorbent eco-friendly semi-interpenetrating network based on cross-linked poly acrylic acid/xanthan gum/graphene oxide (PAA/XG/GO): characterization and dye removal ability. Int J Biol Macromol 152:884–893

[11] Zhou Y, Lu J, Zhou Y, Liu Y (2019) Recent advances for dyes removal using novel adsorbents: a review. Environ Pollut 252:352–365

[12] Zambare R, Song X, Bhuvana S, Antony Prince JS, Nemade P (2017) Ultrafast dye removal using ionic liquid-graphene oxide sponge. ACS Sustain Chem Eng 5:6026–6035

[13] Hu K, Xie X, Szkopek T, Cerruti M (2016) Understanding hydrothermally reduced graphene oxide hydrogels: from reaction products to hydrogel properties. Chem Mater 28:1756–1768

[14] Song S, Ma Y, Shen H, Zhang M, Zhang Z (2015) Removal and recycling of ppm levels of methylene blue from an aqueous solution with graphene oxide. RSC Adv 5:27922–27932

[15] Sitko R, Turek E, Zawisza B, Malicka E, Talik E, Heimann J, Gagor A, Feist B, Wrzalik R (2013) Adsorption of divalent metal ions from aqueous solutions using graphene oxide. Dalton Trans 42:5682–5689

[16] Boukhalfa N, Boutahala M, Djebri N, Idris A (2019) Kinetics, thermodynamics, equilibrium isotherms, and reusability studies of cationic dye adsorption by magnetic alginate/oxidized multiwalled carbon nanotubes composites. Int J Biol Macromol 123:539–548

[17] Yang X, Li Y, Du Q, Sun J, Chen L, Hu S, Wang Z, Xia Y, Xia L (2015) Highly effective removal of basic fuchsin from aqueous solutions by anionic polyacrylamide/graphene oxide aerogels. J Colloid Interface Sci 453:107–114

[18] Chen L, Li Y, Du Q, Wang Z, Xia Y, Yedinak E, Lou J, Ci L (2017) High performance agar/graphene oxide composite aerogel for methylene blue removal. Carbohydr Polym 155:345–353

[19] Yan M, Huang W, Li Z (2019) Chitosan cross-linked graphene oxide/lignosulfonate composite aerogel for enhanced adsorption of methylene blue in water. Int J Biol Macromol 136:927–935

[20] Sashkina KA, Gurikov PA, Ayupov AB, Smirnova I, Parkhomchuk EV (2018) Zeolite/silica aerogel composite monoliths and microspheres. Micropor Mesopor Mat 263:106–112

[21] Daniel-da-Silva AL, Salgueiro AM, Creaney B, Oliveira-Silva R, Silva NJO, Trindade T (2015) Carrageenan-grafted magnetite nanoparticles as recyclable sorbents for dye removal. J Nanopart Res 17:302

[22] Soedjak HS (2002) Colorimetric determination of carrageenans and other anionic hydrocolloids with methylene blue. Anal Chem 66:4514–4518

[23] Liu C, Omer AM, Ouyang XK (2018) Adsorptive removal of cationic methylene blue dye using carboxymethyl cellulose/κ-carrageenan/activated montmorillonite composite beads: Isotherm and kinetic studies. Int J Biol Macromol 106:823–833

[24] Duman O, Tunc S, Polat TG, Bozoglan BK (2016) Synthesis of magnetic oxidized multiwalled carbon nanotube-kappa-carrageenan-Fe_3O_4 nanocomposite adsorbent and its application in cationic Methylene Blue dye adsorption. Carbohydr Polym 147:79–88

[25] Qu W, He D, Huang H, Guo Y, Tang Y, Song R (2020) Characterization of amino-crosslinked hypromellose and its adsorption characteristics for methyl orange from water. J Mater Sci 55:7268–7282. https://doi.org/10.1007/s10853-020-04517-6

[26] Pu W, Song Z, Yan J, Xu H, Ji H, Yuan S, Li H (2019) Preparation of oxygen-deficient 2D WO_{3-x} nanoplates and their adsorption behaviors for organic pollutants: equilibrium and kinetics modeling. J Mater Sci 54:12463–12475

[27] Ersan G, Kaya Y, Ersan MS, Apul OG, Karanfil T (2019) Adsorption kinetics and aggregation for three classes of carbonaceous adsorbents in the presence of natural organic matter. Chemosphere 229:515–524

[28] Langmuir I (1918) The adsorption of gases on plane surfaces of glass, mica and platinum. J Am Chem Soc 40:1361–1403

[29] Freundlich HMF (1906) Over the adsorption in solution. J Phys Chem A 57:385–471

[30] Abdulla NK, Siddiqui SI, Tara N, Hashmi AA, Chaudhry SA (2019) Psidium guajava leave-based magnetic nanocomposite γ-Fe_2O_3@GL: a green technology for methylene blue removal from water. J Environ Chem Eng 7:103423

[31] Tran HN, You SJ, Hosseini-Bandegharaei A, Chao HP (2017) Mistakes and inconsistencies regarding adsorption of contaminants from aqueous solutions: a critical review. Water Res 120:88–116

[32] Yang ST, Chang Y, Wang H, Liu G, Chen S, Wang Y, Liu Y, Cao A (2010) Folding/aggregation of graphene oxide and its application in Cu^{2+} removal. J Colloid Interface Sci 351:122–127

[33] Morimune S, Nishino T, Goto T (2012) Poly (vinyl alcohol)/graphene oxide nanocomposites prepared by a simple eco-process. Polym J 44:1056–1063

[34] Paşcalău V, Popescu V, Popescu GL, Dudescu MC, Borodi G, Dinescu A, Perhaiţa I, Paul M (2012) The alginate/κ-carrageenan ratio's influence on the properties of the cross-linked composite films. J Alloy Compd 536:S418–S423

[35] Nanaki S, Karavas E, Kalantzi L, Bikiaris D (2010) Miscibility study of carrageenan blends and evaluation of their effectiveness as sustained release carriers. Carbohydr Polym 79:1157–1167

[36] Rasool N, Yasin T, Heng JYY, Akhter Z (2010) Synthesis and characterization of novel pH-, ionic strength and temperature-sensitive hydrogel for insulin delivery. Polymer 51:1687–1693

[37] Prado-Fernández J, Rodriguez-Vazquez JA, Tojo E, Andrade JM (2003) Quantitation of κ-, ι- and λ-carrageenans by mid-infrared spectroscopy and PLS regression. Analytica Chimica Acta 480:23–37

[38] Wu Z, Huang W, Shan X, Li Z (2020) Preparation of a porous graphene oxide/alkali lignin aerogel composite and its adsorption properties for methylene blue. Int J Biol Macromol 143:325–333

[39] Lokhande KD, Pethsangave DA, Kulal DK, Some S (2020) Remediation of toxic dye pollutants by using graphene-based adsorbents. Chem Select 5:8062–8073

[40] Zhang D-D, Zu S-Z, Han B-H (2009) Inorganic-organic hybrid porous materials based on graphite oxide sheets. Carbon 47:2993–3000

[41] Kong Y, Wang L, Ge Y, Su H, Li Z (2019) Lignin xanthate resin-bentonite clay composite as a highly effective and low-cost adsorbent for the removal of doxycycline hydrochloride antibiotic and mercury ions in water. J Hazard Mater 368:33–41

[42] Prasad K, Kaneko Y, Kadokawa J (2009) Novel gelling systems of kappa-, iota- and lambda-carrageenans and their composite gels with cellulose using ionic liquid. Macromol Biosci 9:376–382

[43] Wang J, Zhao G, Jing L, Peng X, Li Y (2015) Facile self-assembly of magnetite nanoparticles on three-dimensional graphene oxide-chitosan composite for lipase immobilization. Biochem Eng J 98:75–83

[44] Stankovich S, Dikin DA, Piner RD, Kohlhaas KA, Kleinhammes A, Jia Y, Wu Y, Nguyen ST, Ruoff RS (2007) Synthesis of graphene-based nanosheets via chemical reduction of exfoliated graphite oxide. Carbon 45:1558–1565

[45] Qi Y, Yang M, Xu W, He S, Men Y (2017) Natural polysaccharides-modified graphene oxide for adsorption of organic dyes from aqueous solutions. J Colloid Interface Sci 486:84–96

[46] Inbaraj BS, Chen BH (2011) Dye adsorption characteristics of magnetite nanoparticles coated with a biopolymer poly (gamma-glutamic acid). Bioresour Technol 102:8868–8876
[47] Rocher V, Bee A, Siaugue JM, Cabuil V (2010) Dye removal from aqueous solution by magnetic alginate beads cross-linked with epichlorohydrin. J Hazard Mater 178:434–439
[48] Qin L, Ge Y, Deng B, Li Z (2017) Poly (ethylene imine) anchored lignin composite for heavy metals capturing in water. J Taiwan Inst Chem E 71:84–90
[49] Abdellah AR, Abdelhamid HN, El-Adasy A-BAAM, Atalla AA, Aly KI (2020) One-pot synthesis of hierarchical porous covalent organic frameworks and two-dimensional nano-materials for selective removal of anionic dyes. J Environ Chem Eng 8:104054
[50] Liu Y, Luo C, Sun J, Li H, Sun Z, Yan S (2015) Enhanced adsorption removal of methyl orange from aqueous solution by nanostructured proton-containing δ-MnO_2. J Mater Chem A 3:5674–5682
[51] Ho YS (2006) Review of second-order models for adsorption systems. J Hazard Mater 136:681–689
[52] Tang S, Xia D, Yao Y, Chen T, Sun J, Yin Y, Shen W, Peng Y (2019) Dye adsorption by self-recoverable, adjustable amphiphilic graphene aerogel. J Colloid Interface Sci 554:682–691
[53] Zhang F, Xue X, Huang X, Yang H (2020) Adsorption and heterogeneous Fenton catalytic performance for magnetic Fe_3O_4/reduced graphene oxide aerogel. J Mater Sci 55:15695–15708
[54] Kaur K, Jindal R, Meenu (2019) Self-assembled GO incorporated CMC and Chitosan-based nanocomposites in the removal of cationic dyes. Carbohydr Polym 225:115245
[55] Ren F, Li Z, Tan WZ, Liu XH, Sun ZF, Ren PG, Yan DX (2018) Facile preparation of 3D regenerated cellulose/graphene oxide composite aerogel with high-efficiency adsorption towards methylene blue. J Colloid Interface Sci 532:58–67
[56] Liu J, Chu H, Wei H, Zhu H, Wang G, Zhu J, He J (2016) Facile fabrication of carboxymethyl cellulose sodium/-graphene oxide hydrogel microparticles for water purification. RSC Adv 6:50061–50069
[57] Dai H, Zhang Y, Ma L, Zhang H, Huang H (2019) Synthesis and response of pineapple peel carboxymethyl cellulose-g-poly (acrylic acid-co-acrylamide)/graphene oxide hydrogels. Carbohydr Polym 215:366–376
[58] Eltaweil AS, Elgarhy GS, El-Subruiti GM, Omer AM (2020) Carboxymethyl cellulose/carboxylated graphene oxide composite microbeads for efficient adsorption of cationic methylene blue dye. Int J Biol Macromol 154:307–318
[59] Teli MD, Nadathur GT (2018) Adsorptive removal of acid yellow 17 (an anionic dye) from water by novel ionene chloride modified electrospun silica nanofibres. J Environ Chem Eng 6:7257–7272
[60] Dai J, Xie A, Zhang R, Ge W, Chang Z, Tian S, Li C, Yan Y (2018) Scalable preparation of hierarchical porous carbon from lignin for highly efficient adsorptive removal of sulfamethazine antibiotic. J Mol Liq 256:203–212
[61] Saxena R, Saxena M, Lochab A (2020) Recent progress in nanomaterials for adsorptive removal of organic contaminants from wastewater. Chem Select 5:335–353
[62] Dai L, Zhu W, He L, Tan F, Zhu N, Zhou Q, He M, Hu G (2018) Calcium-rich biochar from crab shell: An unexpected super adsorbent for dye removal. Bioresour Technol 267:510–516